

Effect of Visible Light Illumination on the Atmospheric Corrosion Behaviors of Pure Copper Pre-deposited with NaCl Particles

Xingchen Liu^{1,2,3}, Zhuoyuan Chen^{1,3,*}, Jian Hou³, Jiarun Li¹, Xiaoying Sun¹, Mingxian Sun³

¹ Key Laboratory of Marine Environmental Corrosion and Bio-fouling, Institute of Oceanology, Chinese Academy of Sciences, 7 Nanhai Road, Qingdao 266071, China

² University of Chinese Academy of Sciences, 19 (Jia) Yuquan Road, Beijing 100039, China

³ State Key Laboratory for Marine Corrosion and Protection, Luoyang Ship Material Research Institute, Wenhai Road, Qingdao 266237, China

*E-mail: zychen@qdio.ac.cn

Received: 16 March 2018 / *Accepted:* 11 August 2018 / *Published:* 5 November 2018

Metallic materials serving in the atmospheric environments are usually exposed to solar light illumination. The aim of this work is to determine how the visible light illumination affects the atmospheric corrosion of copper. The mass gains and mass losses after laboratory exposure at different conditions were obtained, and the corrosion morphologies, corrosion products and the electrochemical/photoelectrochemical properties of the corrosion products were analyzed in the present paper. The visible light illumination significantly promoted the atmospheric corrosion of copper. Due to the photoelectrochemical effect, the corrosion products, which possess n-type semiconductor properties, generate the photoinduced electrons and holes. The photoinduced electrons promote the reduction of the dissolved oxygen in the thin NaCl electrolyte layer on the surface of copper, while the photoinduced holes capture the electrons released from the anodic dissolution of the copper substrate, thus accelerating the atmospheric corrosion process of copper under visible light illumination.

Keywords: Atmospheric corrosion; copper; photoelectrochemical effect; photoinduced current density

1. INTRODUCTION

Atmospheric corrosion behaviors of copper have been widely studied because of the extensive applications of copper in electronic and construction industries [1-5]. In marine environment, NaCl is one of the major influencing factors and has a strong accelerating effect on the atmospheric corrosion of copper due to the strong corrosiveness of chloride ions [6]. Chloride ion reacts with copper to form

copper chloride complex ions and consequently affects the corrosion process, resulting in the formation of copper hydroxyl chloride, which is one of the characteristic corrosion products produced in the chloride-containing environments [7]. Additionally, relative humidity (RH), ozone, carbon dioxide, sulfur dioxide, *etc.*, are also the impact factors to affect the corrosion process of copper exposed in humidified atmosphere, and a lot of investigations have been carried out to study their roles on the atmospheric corrosion of copper [8-12].

In addition to the impact factors mentioned above, light illumination is an important factor affecting the corrosion process of metallic materials. However, the influencing mechanism of light illumination on the corrosion process of metallic materials is often neglected. Currently, there are only a few reports on this subject. Burleigh *et al.* [13] studied the effect of ultraviolet (UV) light illumination on the corrosion of different metals under long-term-exposure experimental conditions, and they found that UV light illumination increased the corrosion rates of the metals, namely, zinc, carbon steel, aluminum, copper and silver. Several studies elucidated that the light illumination would affect the corrosion of metals via the photoelectrochemical effect of the passivation film or corrosion product layer with semiconductor properties [14, 15]. Breslin *et al.* [16] investigated the passivation of the copper alloys and the dissolution of the passivation layer under UV light illumination in chloride-containing solutions, suggesting that UV light will inhibit the dissolution of the passivation layer due to its semiconductor properties. Lin *et al.* [17] reported the effect of UV light illumination, ozone and NaCl on the atmospheric corrosion of copper. They claimed that the corrosion of copper was accelerated intensively by UV light illumination despite in the presence of ozone, and the accelerating effect of UV light illumination was more obvious at a low relative humidity.

These studies mentioned above were all carried out under UV light illumination. It is well known that UV light illumination often leads to the generation of ozone and atomic oxygen [18, 19], which could promote the corrosion of metals and consequently bring some misunderstanding on interpreting the photoinduced corrosion of metals. In the present work, visible light was used as the illumination source, aiming at avoiding the influence of UV-induced ozone and atomic oxygen on the atmospheric corrosion of copper. Therefore, the real influence of the photoelectrochemical effect of the corrosion products with semiconductor properties on the atmospheric corrosion process of copper can be studied. Quantitative NaCl particles were pre-deposited on the copper surface for forming a thin liquid film via deliquescent effect in humidified pure air, and then the laboratory studies on the atmospheric corrosion of copper were carried out both in the dark and under visible light illumination, respectively. The mechanism of the role of visible light illumination on the atmospheric corrosion of copper is also discussed in this paper.

2. EXPERIMENTAL

2.1 Sample preparation

Pure copper samples (99.99%) used for laboratory exposure were of $50 \times 10 \times 1$ mm³ in size. Each sample was ground by SiC papers down to 3000 grit successively, and then polished with

diamond grinding paste down to 1 μm . Furthermore, each sample was ultrasonically cleaned in acetone for 5 minutes. The cleaned samples were then stored in a desiccator over silica gel for approximately 24 hours before exposure. NaCl particles were deposited by well distributing small quantities of NaCl saturated ethanol solution onto the copper surface using a transfer pipette [20]. The deposition amount of NaCl particles on the samples was $15 \mu\text{g cm}^{-2}$, which is used to imitate the natural settlement of salt particles on the surface of copper in marine atmosphere.

2.2 Laboratory exposure

The apparatus used for laboratory exposure has been described detailedly in a previous paper from the authors' laboratory [14]. A pure airflow generated by an air pump, passed through the exposure glass chamber ($50 \times 40 \times 30 \text{ cm}^3$ in size) with a velocity of 30 mL min^{-1} . The flowing air was bubbled in a saturated K_2SO_4 solution to control the RH of the exposure chamber. The exposure temperature in the chamber sustained at $25 \pm 1^\circ\text{C}$. Pre-deposited NaCl particles would occur deliquescence reaction in the exposure chamber, which would make the surfaces of the copper samples uniformly covered with a thin electrolyte layer. The cold light LED, which was basically free of ultraviolet and infrared lights, was adopted as the light illumination source with optical intensity of approximately 0.590 mW cm^{-2} . All samples were exposed at 97% RH and $25 \pm 1^\circ\text{C}$ for 1, 2 and 4 weeks in the dark or under visible light illumination, respectively. Nine parallel samples were used in each exposure condition. After exposure, the corroded copper samples were stored in a desiccator for further analyses.

2.3 Mass gain and mass loss measurements

The corrosion of copper samples after laboratory exposure was determined quantitatively by measuring the increase and decrease of the weights of the copper samples. In order to distinguish the samples in different exposure environments, the samples exposed in the dark and under visible light are denoted as Cu_D and Cu_V , respectively. Consequently, the samples experienced different exposure times of 1, 2 and 4 weeks are denoted as $\text{Cu}_\text{D-1}$, $\text{Cu}_\text{D-2}$, $\text{Cu}_\text{D-4}$ and $\text{Cu}_\text{V-1}$, $\text{Cu}_\text{V-2}$, $\text{Cu}_\text{V-4}$, respectively. Mass gain equals to the mass after laboratory exposure minus that of the samples after deposited with NaCl particles, and the mass loss equals to the mass of the sample before depositing NaCl particles minus that of the sample after removing the corrosion products. Corrosion products were removed by pickling the corroded copper samples in sulfaminic acid according to the International Standard (ISO 8407:2009(E)). A microbalance (Sartorius CPA 26P, Germany) with a $4\text{-}\mu\text{g}$ specified precision was used for the weight measurements. The detailed description has been reported in the previous work from the authors' laboratory [14].

2.4 Characterizations of the corrosion products

The corrosion morphologies of the copper samples after laboratory exposure were observed using a scanning electron microscope (SEM, TM3000, Hitachi Co., Japan). The phases of the

corrosion products were identified by X-ray diffraction (XRD, Ultima IV, Rigaku Co., Japan). And the XRD pattern measurements with a scanning range from 10° to 80° were carried out on an X'Pert PRO diffractometer (Cu K α radiation, 1.5418 Å). Besides, Fourier transform infrared spectra (FT-IR, Nicolet IS10, Thermo Fisher Scientific Co., USA) were used to identify the corrosion products, which were obtained in the transmission mode by adding 128 interferograms at resolution of 4 cm^{-1} using the KBr pellet method.

2.5 Electrochemical measurements

A PARSTAT 4000 Electrochemical Workstation (Princeton Applied Research, Ametek, USA) was employed to perform the electrochemical tests using a traditional three-electrode cell system. The 5.2 wt% NaCl solution was adopted as the electrolyte because the deposited NaCl particles on the surface of copper would absorb moisture from the ambient environment and form an electrolyte layer with a NaCl concentration of 5.2 wt% according to the abovementioned experimental condition [21]. A platinum foil and a Ag/AgCl (saturated by KCl) electrode served as the counter and reference electrodes, respectively. The experimental light source was a 300-W Xe arc lamp (PLS-SXE300, Beijing Changtuo Co. Ltd., China), and the visible light was generated using a 420 nm cut off filter to get rid of the light with the wavelengths less than 420 nm. In order to determine the semiconductor properties of the corrosion products, Mott-Schottky plots were conducted in the dark at the potential range from -0.25 to 0.35 V (vs. Ag/AgCl) with AC voltage magnitude of 10 mV at a constant frequency of 1000 Hz . The corrosion product thin-film photoelectrodes were fabricated by collecting the corrosion products formed on copper and then evenly depositing them onto the fluorine-doped tin oxide (FTO) conductive glass with the work geometric area of 1 cm^2 . The linear polarization curves were obtained in the dark at the potential range of -10 to $+10\text{ mV}$ (vs. corrosion potential) with a scan rate of 0.25 mV s^{-1} . The electrochemical impedance spectroscopy (EIS) measurements were performed both in the dark and under visible light illumination with $\pm 5\text{ mV}$ disturbing amplitude sinusoidal voltage (frequency range of 100 kHz to 0.1 Hz) at open circuit potential (OCP). The working electrodes for the linear polarization and EIS tests were the corroded copper samples with the test geometric area of 1 cm^2 by sealing with silicone rubber.

2.6 Photoelectrochemical measurements

The photoelectrochemical measurements, including the photoinduced variations of the OCPs of the corroded copper samples, and the photoinduced variations of the current densities of the galvanic coupling of the corrosion product thin-film photoelectrodes and the bare copper electrode, were performed under intermittent visible light illumination in 5.2 wt% NaCl solution using a CHI660D Electrochemical Workstation (Shanghai Chenhua Instrument Co., Ltd., China). A platinum foil and a Ag/AgCl (saturated by KCl) electrode acted as the counter and reference electrodes, respectively. The measurements were done without any applied polarization. The geometric area of the working electrode is 1 cm^2 . More details of the photoelectrochemical measurements could be seen in the

previous work from the authors' laboratory [22]. If not specified, these measurements were repeated 3-6 times to ensure the reproducibility. The reagents used in this work were of analytical purity class and the electrolyte was prepared with deionized water.

3. RESULTS AND DISCUSSION

3.1 Analyses of the mass changes and corrosion rates

Figure 1 shows the mass gains and mass losses of pure copper samples after laboratory exposure at different conditions. Both the mass gains and mass losses of the copper samples increase with the exposure time despite the visible light illumination, manifesting that the corrosion keeps on proceeding with exposure time. Within the same exposure period, the mass gains and mass losses of the samples exposed under visible light illumination are much larger than those of the samples exposed in the dark. As shown in Figure 1, the ratio of the mass loss obtained under visible light illumination to that obtained in the dark after 1, 2 and 4 weeks of exposure are 3.58, 2.80 and 2.37, respectively, demonstrating that the visible light illumination dramatically accelerates the atmospheric corrosion of copper.

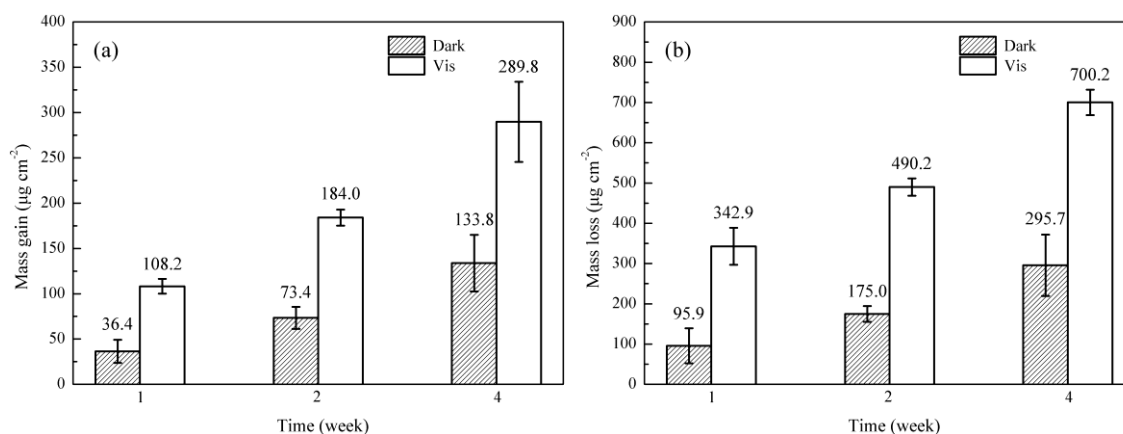


Figure 1. Mass gains (a) and mass losses (b) of copper samples pre-deposited with $15 \mu\text{g cm}^{-2}$ NaCl particles and after 1, 2, and 4 weeks of laboratory exposure in the dark and under visible light illumination in humidified pure air with 97% RH at $25 \text{ }^\circ\text{C}$.

Figure 2 illustrates the average corrosion rates derived from the mass losses data as a function of exposure time. The average corrosion rates decrease with exposure time for both the Cu_D and Cu_V samples. This could be due to the accumulation of the atmospheric corrosion products on the copper surface which hinder the mass transfer processes of the anodic/cathodic reactions. Besides, the average corrosion rates of the Cu_D samples are much lower than those of the Cu_V samples throughout the whole exposure period, further validating that the visible light illumination would significantly promote the atmospheric corrosion of copper.

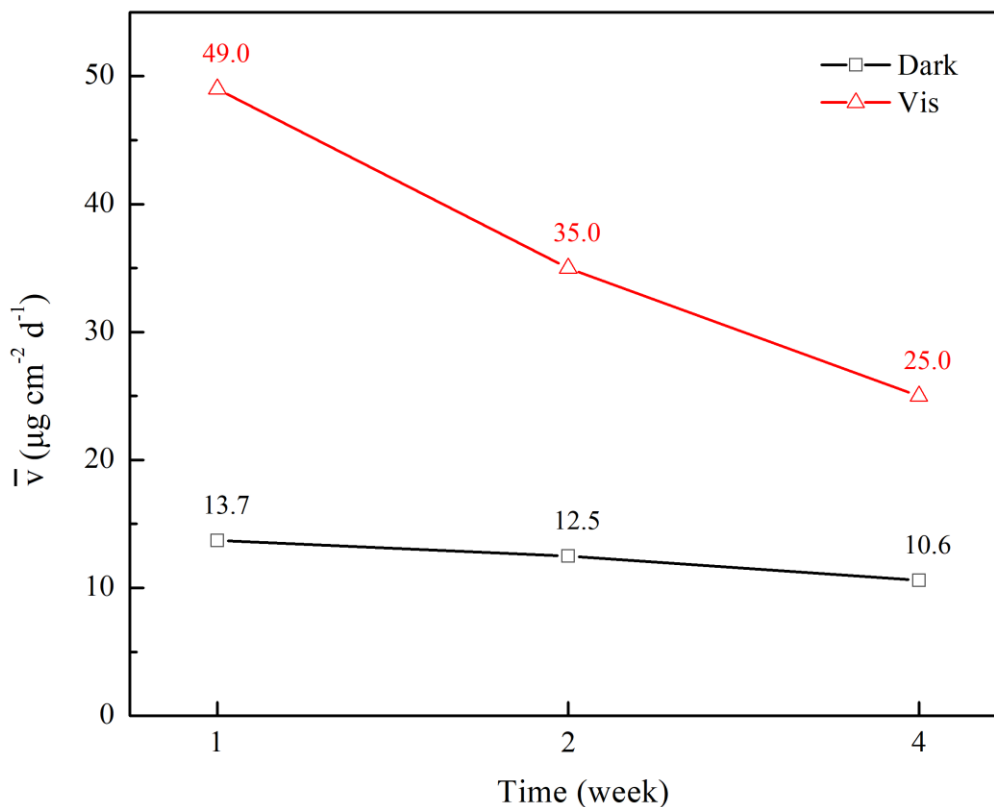


Figure 2. Average corrosion rates of the copper samples derived from the mass losses data as a function of exposure time.

3.2 Characterization of the corrosion products

The corrosion morphologies of the copper samples after 1, 2 and 4 weeks of exposure are depicted in Figure 3, and the insets are the SEM images at higher magnifications. The amount of corrosion products increases with the increase of the exposure time both with and without visible light illumination by comparing the images shown in Figure 3. Meanwhile, the amount of corrosion products exposed in the dark is less than that under visible light illumination over the same exposure period, implying a promoted corrosion induced by the visible light illumination. Besides, the morphologies of the corrosion products between the samples with and without illumination are quite different. In the dark, the granule-like and needle-like corrosion products are found on the surface after 1 week of exposure. Relatively, only the needle-like corrosion products are observed after 2 and 4 weeks of exposure. Under visible light illumination, both the granule-like and needle-like corrosion products appear on the surfaces of the copper samples throughout the whole exposure period. In addition, the corrosion products are more compact under visible light illumination than those in the dark over the same exposure period. As shown in Figure 3, the corrosion products of copper samples exposed under visible light illumination are of great coverage ratios on the surface in compact way, hindering the electrolyte and oxidants, such as oxygen, from contacting with copper substrate directly, which is believed to alleviate the corrosion in literature [23-25].

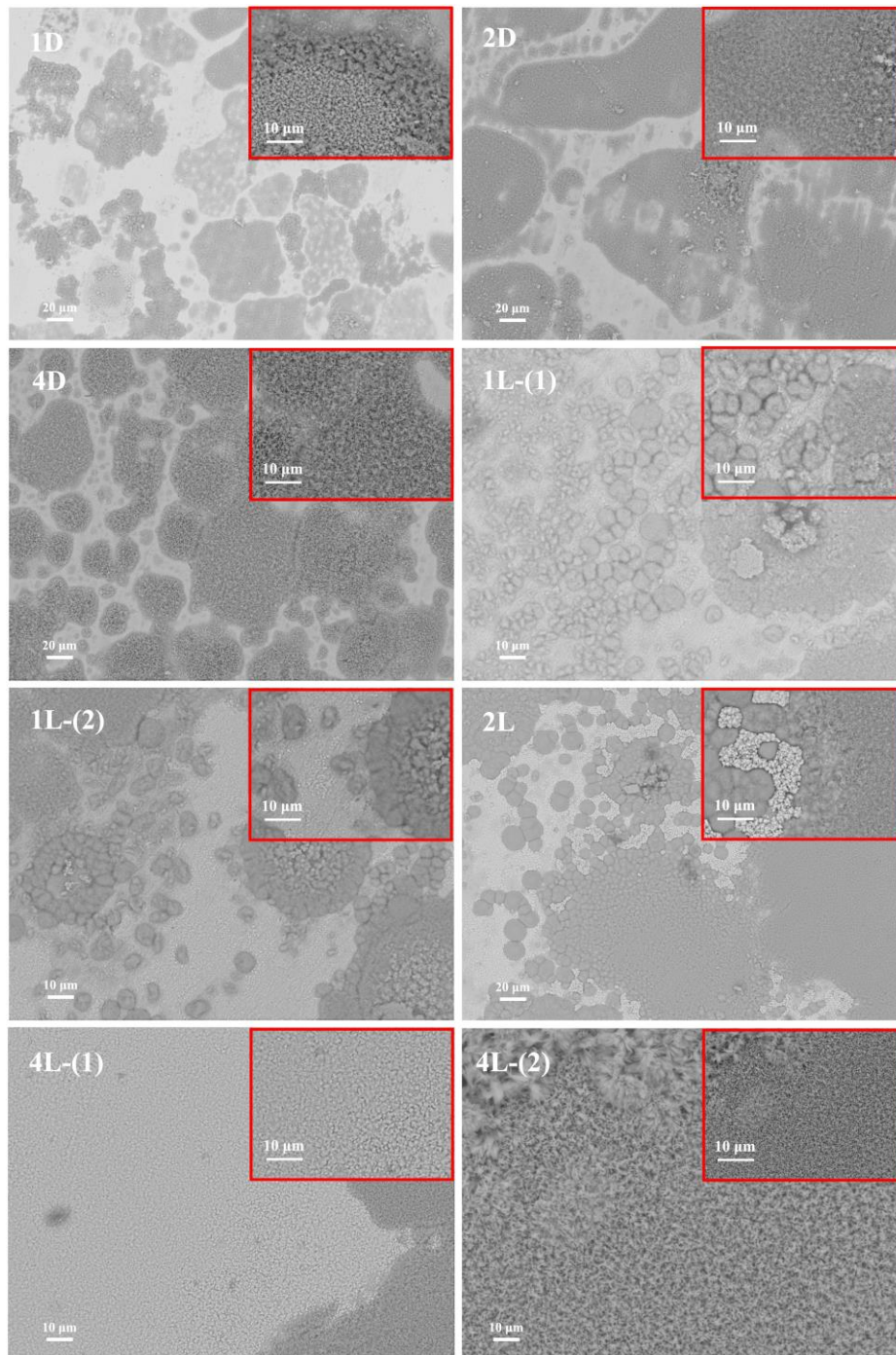


Figure 3. SEM images of the corrosion products formed on the copper surface pre-deposited with $15 \mu\text{g cm}^{-2}$ NaCl particles and after 1, 2 and 4 weeks of exposure to humidified pure air with 97% RH at 25°C in the dark and under visible light illumination.

XRD patterns of the corrosion products formed at different exposure conditions are shown in Figure 4. The major diffraction peaks attributed to the copper substrate and the crystalline cuprite (Cu_2O), indicating that Cu_2O is the main corrosion product [26]. Besides, the malachite ($\text{Cu}_2(\text{OH})_2\text{CO}_3$) peaks [27, 28] were also detected at the XRD spectra of the copper samples after 2 and 4 weeks of exposure under visible light illumination.

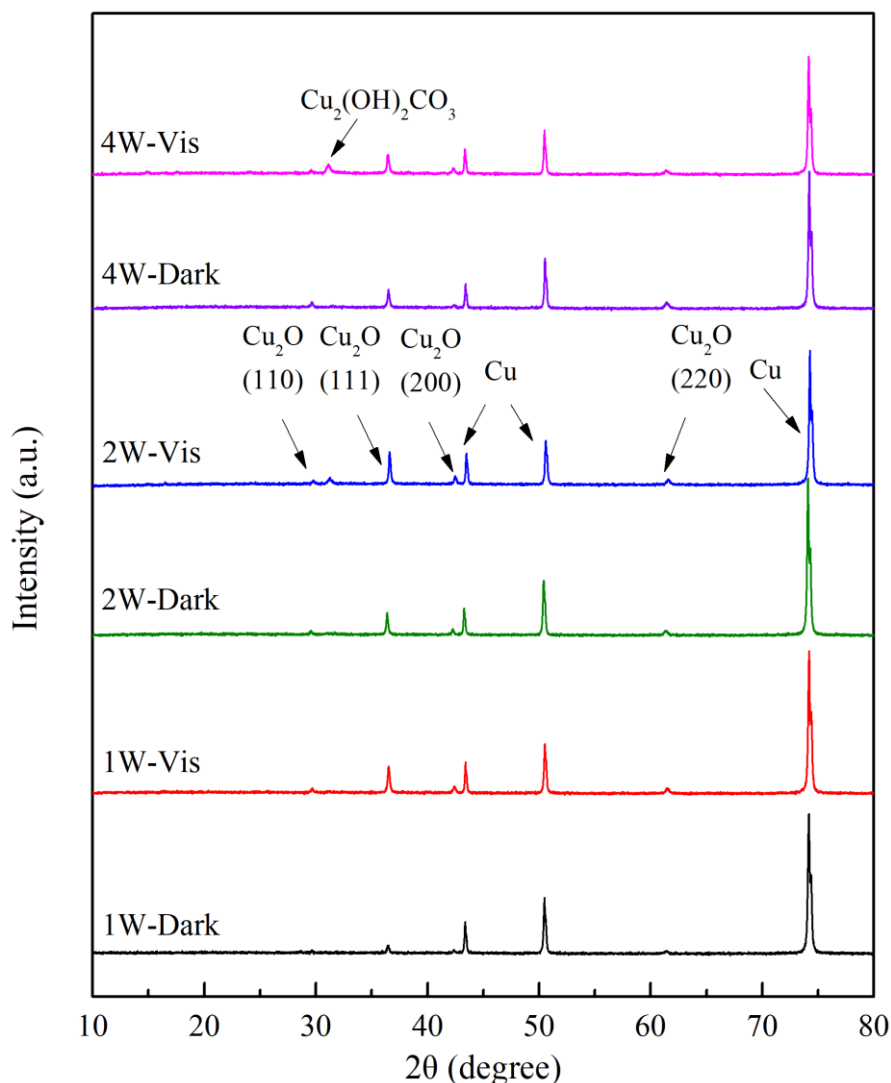


Figure 4. XRD patterns of the corroded copper after 1, 2 and 4 weeks of exposure in the dark and under visible light illumination in humidified pure air with 97% RH at 25 °C.

Figure 5 shows the FT-IR transmission spectra of the corrosion products formed at different exposure conditions. The presence of Cu_2O , $\text{Cu}_2(\text{OH})_3\text{Cl}$ and $\text{Cu}_2(\text{OH})_2\text{CO}_3$ in the corrosion products can be obtained from the spectra depicted in Figure 5. The peak at 623 cm^{-1} is characterized as Cu_2O [29]. The presence of $\text{Cu}_2(\text{OH})_3\text{Cl}$ cannot be identified by those peaks ranging from 3600 cm^{-1} to 3200 cm^{-1} because the stretching vibrations of OH induced by $\text{Cu}_2(\text{OH})_3\text{Cl}$ or by H_2O in the ambient atmosphere could not be clearly distinguished at this wavenumber range [23, 30]. Nonetheless, the peaks at 985 and 920 cm^{-1} correspond to the bending vibrations of Cu-O-H from $\text{Cu}_2(\text{OH})_3\text{Cl}$, and the characteristic peak of $\text{Cu}_2(\text{OH})_3\text{Cl}$ at 520 cm^{-1} also verifies the presence of $\text{Cu}_2(\text{OH})_3\text{Cl}$ in the corrosion products [31, 32]. The peaks at 1501 , 1425 and 1391 cm^{-1} correspond to the characteristic stretching vibrations of carbonate. In addition, the peaks at 1102 , 1054 , 878 , 818 and 753 cm^{-1} prove the presence of $\text{Cu}_2(\text{OH})_2\text{CO}_3$ [31, 33] in the corrosion products. CuCl was not detected in this work, which may be due to its low content or transforming to other substances [7, 34].

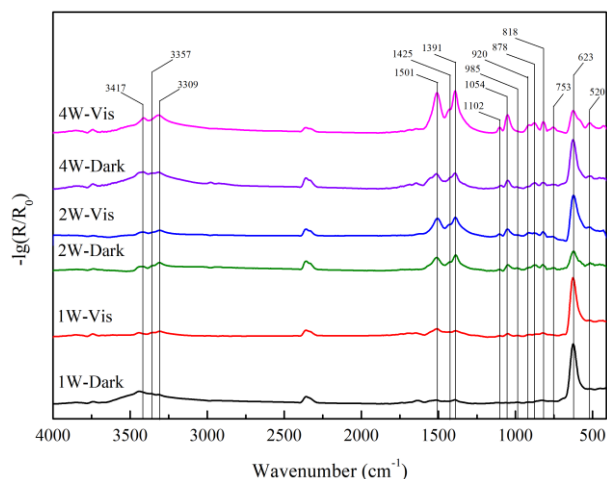


Figure 5. Fourier transform infrared transmission spectra of the corrosion products formed on the surface of copper after 1, 2 and 4 weeks of exposure in the dark and under visible light illumination in humidified pure air with 97% RH at 25 °C.

3.3 Electrochemical behaviors

The Mott-Schottky method is based on the measurement of the space charge capacitances of the semiconductor layer as a function of the applied potentials, which can be used to determine the electric properties of corrosion products with semiconductor properties. Figure 6 depicts the Mott-Schottky plots of the corrosion product thin-film photoelectrodes prepared by the corrosion products formed on the copper samples after exposure at different conditions. As shown in Figure 6, all of the Mott-Schottky plots have positive slopes, indicating that the corrosion products possess n-type semiconductor properties.

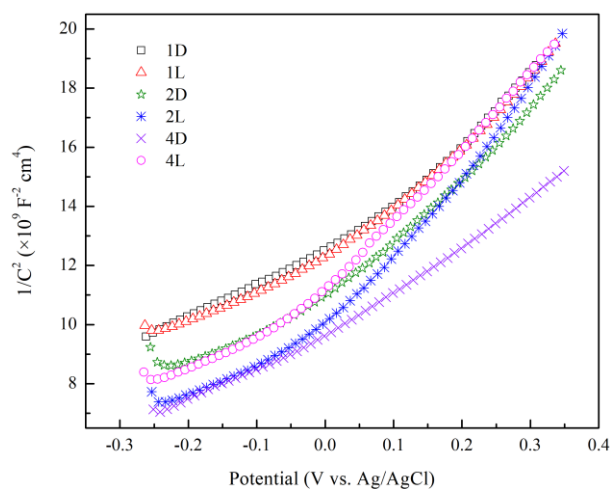


Figure 6. Mott-Schottky plots of the corrosion product thin-film photoelectrodes obtained in 5.2 wt% NaCl solution at 1000 Hz in the dark. The photoelectrodes were prepared using the corroded copper samples after 1, 2 and 4 weeks of exposure in the dark and under visible light illumination in humidified pure air with 97% RH at 25 °C.

According to the experimental results of the XRD patterns and the FT-IR transmission spectra abovementioned, Cu_2O is the major corrosion products. Meanwhile, it is believed that Cu_2O could promote the corrosion under the light illumination due to its n-type semiconductor characteristic in literature [8, 35]. As can be inferred from the above results, the n-type semiconductor properties proved by Mott-Schottky are just those of Cu_2O formed on the surface of copper in chloride-containing environments.

Linear polarization curves, which are normally used to evaluate the polarization resistance, of the corroded copper samples were measured in the dark and the results are presented in Figure 7a. The polarization resistance, R_p , is an important parameter for the corrosion evaluation because $1/R_p$ is proportional to the corrosion current rate. Figure 7b shows the reciprocal of the polarization resistance of the copper samples after exposure at different conditions. As shown in Figure 7b, the corrosion rates ($1/R_p$) of the corroded copper samples decrease with exposure time due to the accumulation of the corrosion products with the increase of exposure time. The accumulated corrosion products can provide some protective effects for the copper substrate [36], and the accumulation of the corrosion products on the copper surface is believed to resist the electrolyte from penetrating into and hinder the diffusion of the corrosion reactants and products, consequently alleviating the corrosion of the copper samples. On the other hand, the corrosion rates obtained by linear polarization of the corroded copper samples exposed in the dark are correspondingly larger than those exposed under visible light illumination, which is attributed to the larger amount of the corrosion products on the copper samples exposed under light illumination. As discussed above, the Cu_2O product layer would promote the corrosion under light illumination, therefore, the corrosion product layer has dual effects on the corrosion of copper, *i.e.*, promoting corrosion under light illumination or alleviating corrosion by covering on the surface of copper.

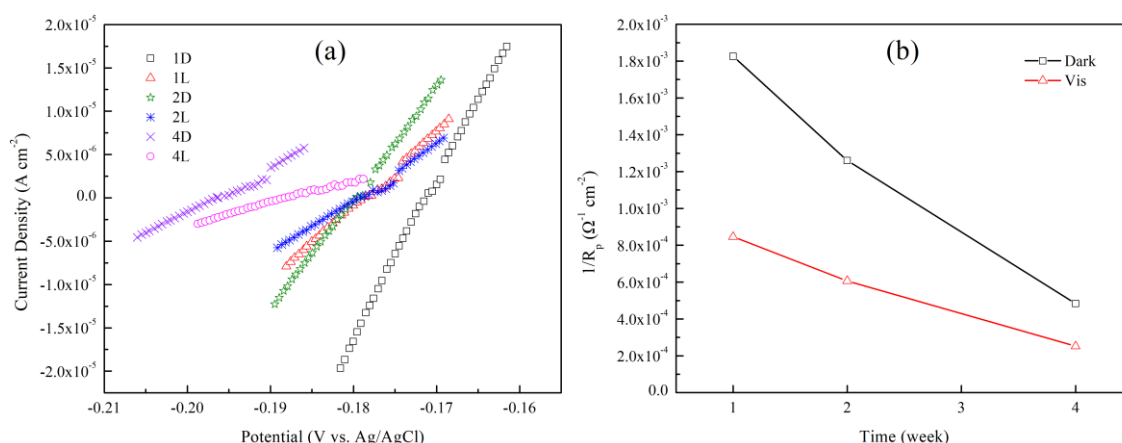


Figure 7. Linear polarization curves (a) and the reciprocal of the polarization resistance (b) of the corroded copper samples after 1, 2 and 4 weeks of exposure in the dark and under visible light illumination in humidified pure air with 97% RH at 25 °C. The measurements were performed in the dark.

EIS is an effective electrochemical measurement which can provide corrosion information in a non-destructive way. The EIS results and corresponding fitting curves of the corroded copper samples measured in 5.2 wt% NaCl and in the dark are presented in Figure 8. Two upward peaks of the copper samples in the Bode diagrams appear at high and low frequencies, respectively, implying that there are two time constants. The equivalent circuit for describing the dynamic process on products covered copper surface in 5.2 wt% NaCl is presented in Figure 9, where R_s represents the solution resistance; R_f and Q_f are the corrosion product resistance and the corrosion product capacitor, respectively; R_{ct} is the charge transfer resistance and Q_{ct} represents the capacitor of the electric double layer. Generally, R_{ct} in the EIS simulated results is inversely proportional to the corrosion rate [37]. The reciprocal of R_{ct} measured in the dark as a function of exposure time is shown in Figure 10, which can represent the changes of the corrosion rates over the exposure time.

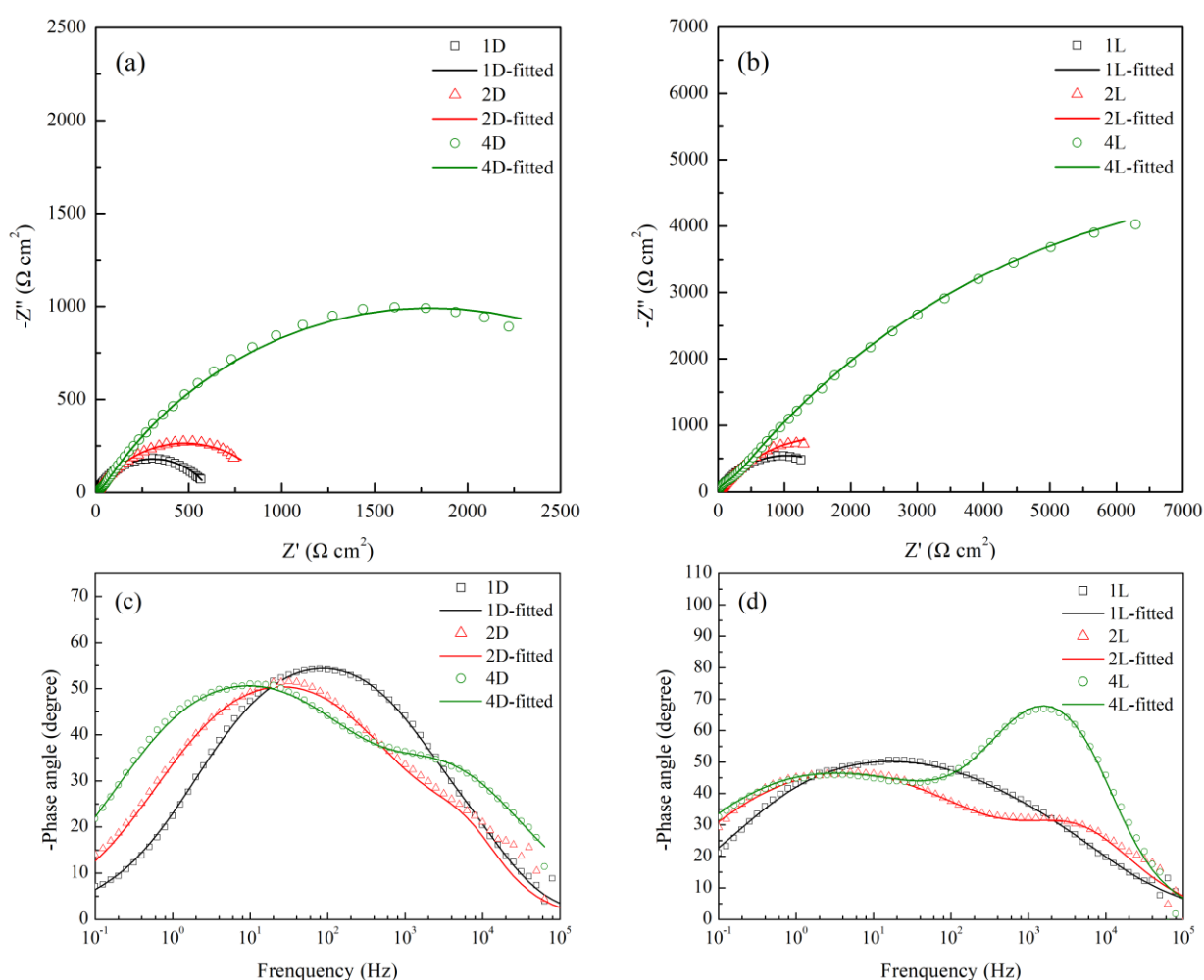


Figure 8. Nyquist plots (a, b) and Bode plots (c, d) of the corroded copper samples after 1, 2 and 4 weeks of exposure in the dark and under visible light illumination in humidified pure air with 97% RH at 25 °C. The measurements were performed in the dark.

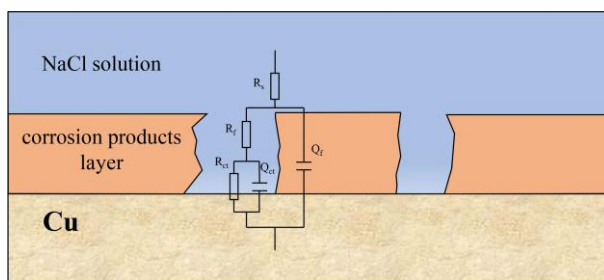


Figure 9. Equivalent circuit for fitting the EIS data shown in Figure 8.

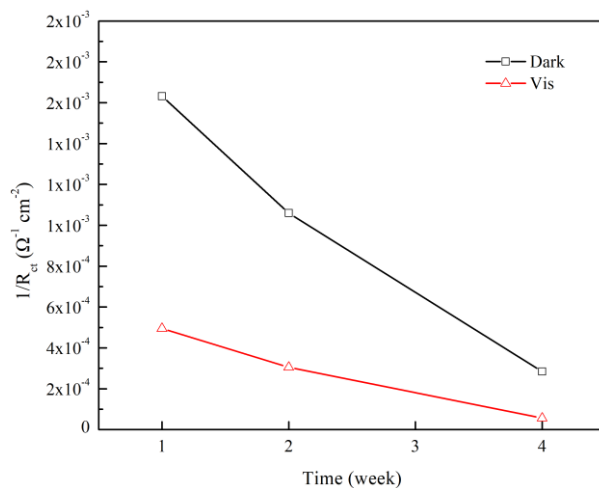


Figure 10. Reciprocal of the charge transfer resistance of the corroded copper samples after 1, 2 and 4 weeks of exposure in the dark and under visible light illumination in humidified pure air with 97% RH at 25 °C.

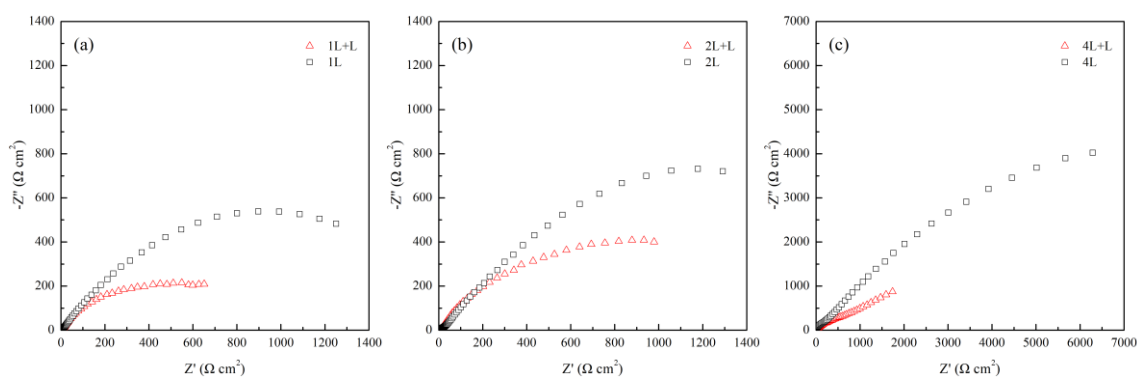


Figure 11. Nyquist plots of the corroded copper samples after 1 (a), 2 (b) and 4 (c) weeks of exposure under visible light illumination. The measurements were performed both in the dark and under visible light illumination.

The variation tendency of the corrosion rates shown in Figure 10 is similar to that shown in Figure 7b. Based on the results shown in Figure 10, the inhibition effect of corrosion products to the copper substrate increases with exposure time. And again, more corrosion products generated on the

corroded copper samples under visible light illumination lead to the lower corrosion rates, as shown in Figure 10 [38].

Figure 11 shows the Nyquist diagrams of the corroded copper samples measured in the dark and under light illumination. The curvature of the curve in the Nyquist diagram measured under the light illumination is noticeably reduced. Due to the photoelectrochemical effect of the corrosion products (Cu_2O) with semiconductor properties under the light illumination, the photoinduced electron-hole pairs would be generated and the free flow of the photoinduced charge carriers would lead to a decrease in the diameter of the semicircle in the Nyquist diagram [39].

3.4 Photoelectrochemical measurements

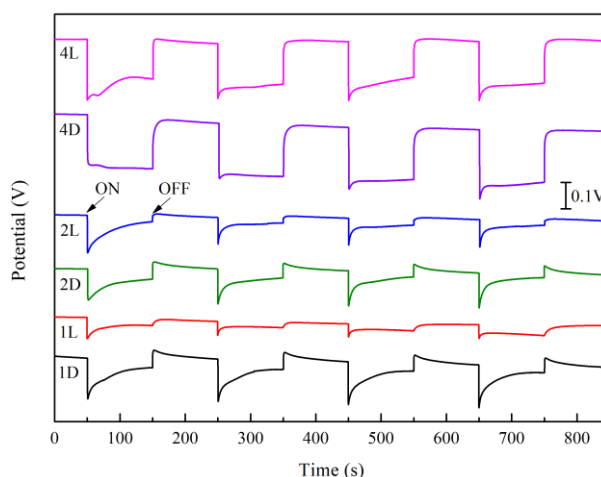


Figure 12. Variations in the open circuit potentials of the corroded copper samples under intermittent visible light on and off. The corroded copper samples were after 1, 2 and 4 weeks of exposure in the dark and under visible light illumination in humidified pure air with 97% RH at 25 °C.

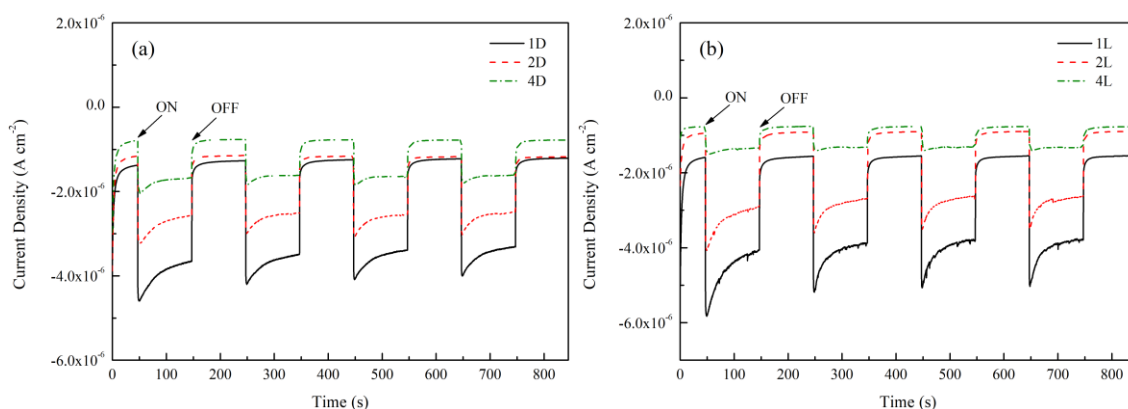
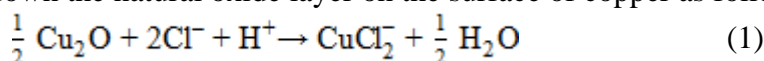


Figure 13. Variations of the current densities of the coupled copper electrode and corrosion product thin-film photoelectrodes under intermittent visible light on and off. The photoelectrodes were prepared using the corroded copper samples after 1, 2 and 4 weeks of exposure in the dark (a) and under visible light illumination (b) in humidified pure air with 97% RH at 25 °C.

Figure 12 shows the visible light induced OCP variations of the corroded copper samples. A two-electrode cell was adopted in the tests and the interval of light on and off was 100 s. As shown in Figure 12, the visible light illumination shifts the OCP towards negative direction for the corroded copper samples. Figure 13 depicts the photoinduced current density-time curves of the bare copper electrode coupled with the corrosion product thin-film photoelectrodes. The negative current densities ranging from -1.0 to $-2.0 \mu\text{A cm}^{-2}$ in the dark were obtained, implying that the electrons flow from the copper electrode to the corrosion product thin-film photoelectrode [40]. Besides, the current densities of the copper electrode coupled with the corrosion product thin-film photoelectrodes increase negatively when the light illumination is on. This result demonstrates intuitively that the photogenerated electrons cannot transfer to the coupled copper electrode. On the contrary, the photogenerated holes directly capture the electrons produced by the anodic dissolution of copper, thus accelerating the atmospheric corrosion process of copper [41]. Therefore, the results shown in Figure 13 provide the experimental evidence for the accelerated atmospheric corrosion of copper under visible light illumination.

3.5 Effect of visible light illumination on the atmospheric corrosion of copper

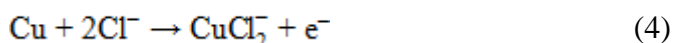
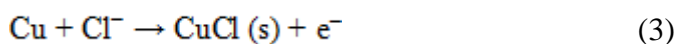
Figure 14 schematically illustrates the corrosion of copper in the dark and under visible light illumination. First of all, the pre-deposited NaCl particles would absorb moisture from the ambient environment and a thin electrolyte layer was formed at the outset. Then, the chloride ions would breakdown the natural oxide layer on the surface of copper as follows [42]:



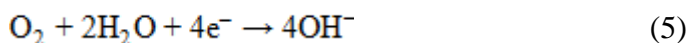
The exposed copper substrate would be oxidized to ions and release electrons because the corrosion of copper in the atmosphere is an electrochemical process, and thus,



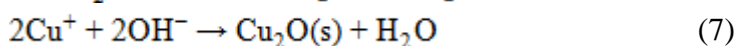
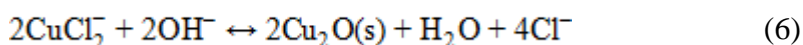
In general, CuCl_2 is the main soluble cuprous chloride complex in 5.2 wt% NaCl solution [43], as a consequence, CuCl and cuprous chloride complex would be generated as the oxidized products of Cu due to the presence of chloride ions [44],



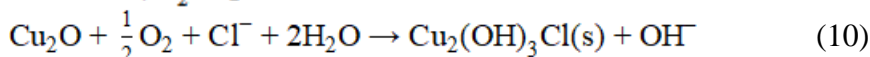
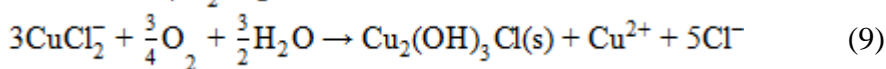
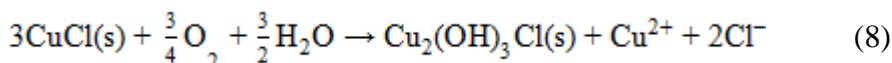
On the other hand, the dissolved oxygen in the thin electrolyte layer proceeds the reduction reaction:



The oxidized products, CuCl_2 and Cu^+ , which are soluble in the solution, could react with OH^- and further be converted to Cu_2O through precipitation reaction [45].



Due to the presence of free chloride ions and dissolved oxygen, copper hydroxyl chloride ($\text{Cu}_2(\text{OH})_3\text{Cl}$) would be generated via further oxidation reactions of CuCl , CuCl_2 and Cu_2O ,



The increasing amount of OH⁻ generated via the cathodic reaction arouses the pH increase of the thin electrolyte layer, which makes the CO₂ in the ambient atmosphere be apt to dissolve. Then, the generated CO₃²⁻ via the dissociation of carbonic acid would facilitate the generation of copper hydroxyl carbonate (Cu₂(OH)₂CO₃) in the corrosion products [42]. It is believed that the corrosion products of copper show a layer-by-layer structure [45], and the inner product layer is mainly of Cu₂O and the loose corrosion product layer outside is comprised of Cu₂(OH)₃Cl and Cu₂(OH)₂CO₃, which are locally distributed above the Cu₂O layer [17,46]. Thus, the corrosion process of copper in the dark can be schematically illustrated in Figure 14a.

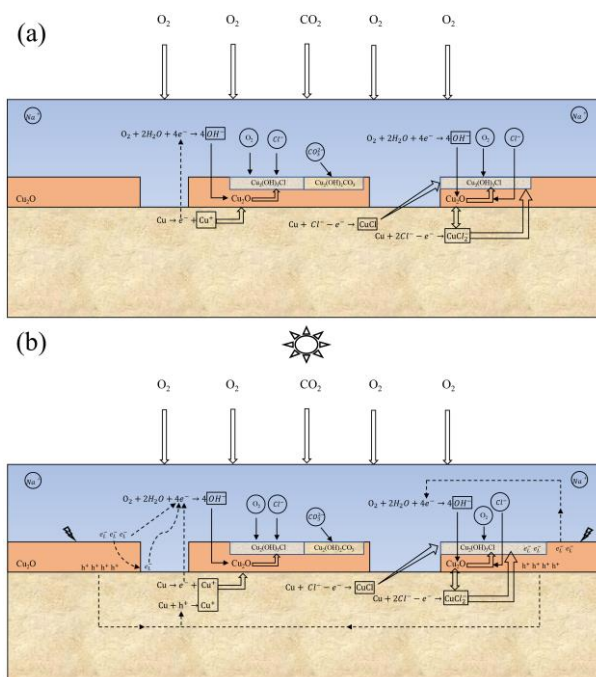
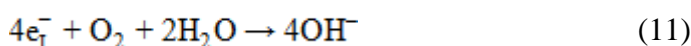


Figure 14. Schematic illustration of the corrosion processes of copper exposed in the dark (a) and under visible light illumination (b).

As shown in Figure 6, the atmospheric corrosion products possess n-type semiconductor properties. Due to the photoelectrochemical effect, the corrosion products with n-type semiconductor properties will generate the photoinduced electrons and holes under visible light illumination. As the results shown in Figure 4 and 5, the atmospheric corrosion products contain Cu₂O, copper hydroxyl chloride (Cu₂(OH)₃Cl) and copper hydroxyl carbonate (Cu₂(OH)₂CO₃). Among these corrosion products, only Cu₂O formed in chloride-containing environments possesses n-type semiconductor properties. The forbidden band gap of Cu₂O is 2.2 eV, indicating that Cu₂O has the photoelectrochemical response ability under visible light illumination and the photoinduced electron-

hole pairs would be generated under visible light illumination. The valence band (VB) potential and the conduction band (CB) potential of Cu₂O are 1.92 and -0.28 V (vs. SHE), respectively. And the Fermi level of the n-type Cu₂O is closed to its CB. For the corroded copper samples, Cu₂O contacts the copper substrate and the thin electrolyte layer directly. The work function of copper is 4.65 eV, and the redox potential of O₂/H₂O is approximately 0.8 V (vs. SHE pH=7). In view of thermodynamics, the potential difference between the CB potential of Cu₂O and the redox potential of O₂/H₂O is larger than that between the CB potential of Cu₂O and the work function of copper. The photoinduced electrons on the CB would easily react with the dissolved oxygen in the NaCl electrolyte. Similarly, the photoinduced holes on the VB could easily react with the copper substrate and the electrons of copper could flow to the semiconductor. The processes mentioned above are proved by the variations of the photoinduced current density shown in Figure 13.

The photoinduced electrons generated under visible light illumination would react with dissolved oxygen in solution as follow,



While, the photoinduced holes are prone to oxidize the copper substrate,



The above reaction (12) promotes the oxidation of copper, and the generated cuprous ion would react with OH⁻ derived from the cathodic reduction to form corrosion products, *i.e.*, Cu₂O under visible light illumination. The corrosion processes of copper under visible light illumination are schematically illustrated in Figure 14b. Due to the reaction rate between the excited electrons and dissolved oxygen in electrolyte is lower than the consumption rate of the photoinduced holes, the photogenerated electrons would accumulate in the corrosion product layer, leading to the negative shift of the OCPs as presented in Figure 12. Besides, the increased potential drop of Cu_{D/V} with the increase of the exposure period, *i.e.*, 1, 2 and 4 weeks under light illumination in Figure 12 may be owing to the increasing amount of the corrosion products, which leads to the increase of the thickness of the corrosion product layer. The electrolyte is more difficult to penetrate into the product layer, which makes more photoinduced electrons to accumulate in the corrosion product layer, leading to higher photoinduced potential drops under visible light illumination.

4. CONCLUSIONS

In this paper, the effect of visible light illumination on the NaCl-induced atmospheric corrosion of pure copper was studied. The copper samples were pre-deposited with 15 μg cm⁻² NaCl particles and subsequently exposed to 97% RH at 25 °C for 1, 2 and 4 weeks. Microgravimetry, XRD, FT-IR spectroscopy, SEM, electrochemical and photoelectrochemical test methods were used for studying the effect of visible light illumination on the atmospheric corrosion process of pure copper.

The main conclusions are drawn as follows:

(1) The visible light illumination significantly promotes the atmospheric corrosion of copper. The atmospheric corrosion rates of copper exposed under visible light illumination are 2.37 to 3.58

times those of copper exposed in the dark, demonstrating that the visible light illumination is an important factor affecting the atmospheric corrosion process of copper.

(2) The atmospheric corrosion products possess n-type semiconductor properties. Due to the photoelectrochemical effect, the corrosion products with n-type semiconductor properties generate the photoinduced electrons and holes. They participate in the corrosion electrochemical reactions, and thus directly affect the atmospheric corrosion of copper.

(3) Visible light illumination affects the corrosion morphologies of copper exposed under atmospheric environments, and the corrosion products formed under visible light illumination are more compact than those formed in the dark.

ACKNOWLEDGEMENTS

This work was financially supported by the National Natural Science Foundation of China (Grant No. 41576114) and Qingdao Innovative Leading Talent Foundation (Grant No. 15-10-3-15-(39)-zch). And this work was also financially supported by State Key Laboratory for Marine Corrosion and Protection, Luoyang Ship Material Research Institute, China (Project No. 614290101011703).

References

1. I. Odnevall, C. Leygraf, *J. Electrochem. Soc.*, 142 (1995) 3682.
2. L. Veleva, S. A. Tomas, E. Marin, A. Cruz-Orea, I. Delgadillo, J. J. Alvarado-Gil, P. Quintana, R. Pomes, F. Sanchez, H. Vargas, L. C. M. Miranda, *Corros. Sci.*, 39 (1997) 1641.
3. A. López-Delgado, E. Cano, J. M. Bastidas, F. A. López, *J. Electrochem. Soc.*, 145 (1998) 4140.
4. W. He, I. O. Wallinder, C. Leygraf, *Water, Air, Soil Pollut. Focus*, 1 (2001) 67.
5. T. H. Merkel, H. J. Groß, W. Werner, T. Dahlke, S. Reicherter, G. Beuchle, S. H. Eberle, *Water Res.*, 36 (2002) 1547.
6. G. Mankowski, J. P. Duthil, A. Giusti, *Corros. Sci.*, 39 (1997) 27.
7. X. Zhang, I. O. Wallinder, C. Leygraf, *Corros. Sci.*, 85 (2014) 15.
8. H. Lin, G. S. Frankel, *J. Electrochem. Soc.*, 160 (2013) C336.
9. S. Oesch, M. Faller, *Corros. Sci.*, 39 (1997) 1505.
10. M. Lenglet, J. Lopitiaux, C. Leygraf, I. Odnevall, M. Carballeira, J. C. Noualhaguet, J. Guinement, J. Gautier, J. Boissel, *J. Electrochem. Soc.*, 142 (1995) 3690.
11. P. Eriksson, L. G. Johansson, H. Strandberg, *J. Electrochem. Soc.*, 140 (1993) 53.
12. N. Boulay, M. Edwards, *Water Res.*, 35 (2001) 683.
13. T. D. Burleigh, C. Ruhe, J. Forsyth, *Corrosion*, 59 (2003) 774.
14. L. Song, X. Ma, Z. Chen, B. Hou, *Corros. Sci.*, 87 (2014) 427.
15. L. Song, Z. Chen, B. Hou, *Corros. Sci.*, 93 (2015) 191.
16. C. B. Breslin, D. D. Macdonald, *Electrochim. Acta*, 44 (1998) 643.
17. H. Lin, G. S. Frankel, *Corros. Eng. Sci. Techn*, 48 (2013) 461.
18. Z. Y. Chen, D. Liang, G. Ma, G. S. Frankel, H. C. Allen, R. G. Kelly, *Corros. Eng. Sci. Techn*, 45 (2013) 169.
19. D. Liang, H. C. Allen, G. S. Frankel, Z. Y. Chen, R. G. Kelly, Y. Wu, B. E. Wyslouzil, *J. Electrochem. Soc.*, 157 (2010) C146.
20. Z. Y. Chen, S. Zakipour, D. Persson, C. Leygraf, *Corrosion*, 60 (2004) 479.
21. Z. Y. Chen, F. Cui, R. G. Kelly, *J. Electrochem. Soc.*, 155 (2008) C360.
22. L. Song, Z. Chen, *Corros. Sci.*, 86 (2014) 318.
23. A. R. Mendoza, F. Corvo, A. Gómez, J. Gómez, *Corros. Sci.*, 46 (2004) 1189.
24. I. O. Wallinder, C. Leygraf, *Corros. Sci.*, 43 (2001) 2379.
25. J. J. S. Rodríguez, F. J. S. Hernández, J. E. G. González, *Corros. Sci.*, 45 (2003) 799.

26. M. Chmielová, J. Seidlerová, Z. Weiss, *Corros. Sci.*, 45 (2003) 883.
27. J. Xu, D. Xue, *J. Phys. Chem. B*, 109 (2005) 17157.
28. K. Wieczorek-Ciurowa, K. Gamrat, K. Fela, *Solid State Ionics*, 164 (2003) 193.
29. G. Poling, *J. Electrochem. Soc.*, 116 (1969) 958.
30. L. Núñez, E. Reguera, F. Corvo, E. González, C. Vazquez, *Corros. Sci.*, 47 (2005) 461.
31. J. Malvault, J. Lopitiaux, D. Delahaye, M. Lenglet, *J. Appl. Electrochem.*, 25 (1995) 841.
32. W. Martens, R. L. Frost, P. A. Williams, *N.Jb. Miner, Abh.*, 178 (2003) 197.
33. M. Schmidt, H. Lutz, *Phys. Chem. Miner.*, 20 (1993) 27.
34. D. de la Fuente, J. Simancas, M. Morcillo, *Corros. Sci.*, 50 (2008) 268.
35. U. Bertocci, *J. Electrochem. Soc.*, 125 (1978) 1598.
36. D. C. Kong, C. F. Dong, Y. H. Fang, K. Xiao, C. Y. Guo, G. He, X. G. Li, *Transactions of Nonferrous Metals Society of China*, 26 (2016) 1721.
37. W. Lorenz, F. Mansfeld, *Corros. Sci.*, 21 (1981) 647.
38. R. Orozco-Cruz, *International Journal of Electrochemical Science*, (2017) 3133.
39. J. Wang, F. Su, W. Zhang, *J. Solid State Electrochem.*, 18 (2014) 2921.
40. Y. Y. Bu, J. P. Ao, *Green Energy & Environment*, 2 (2017) 331.
41. W. Zhang, H. Guo, H. Sun, R. Zeng, *Appl. Surf. Sci.*, 410 (2017) 547.
42. H. Strandberg, L. G. Johansson, *J. Electrochem. Soc.*, 145 (1998) 1093.
43. G. Faita, G. Fiori, D. Salvatore, *Corros. Sci.*, 15 (1975) 383.
44. S. Bordbar, M. Alizadeh, M. Iranmanesh, *Journal of Failure Analysis and Prevention*, 17 (2017) 1139.
45. G. Kear, B. D. Barker, F. C. Walsh, *Corros. Sci.*, 46 (2004) 109.
46. V. Araban, M. Kahram, D. Rezakhani, *Corros. Eng. Sci. Techn*, 51 (2016) 498.